# Flow and mixing dynamics of phasetransforming multicomponent fluids

Cite as: Appl. Phys. Lett. **115**, 104101 (2019); https://doi.org/10.1063/1.5109889 Submitted: 13 May 2019 . Accepted: 19 August 2019 . Published Online: 03 September 2019

Saikat Mukherjee 🗓, and Hector Gomez







### **ARTICLES YOU MAY BE INTERESTED IN**

Enhancement of terahertz emission by a preformed plasma in liquid water Applied Physics Letters 115, 101101 (2019); https://doi.org/10.1063/1.5119812

Optomechanical spring enhanced mass sensing

Applied Physics Letters 115, 101103 (2019); https://doi.org/10.1063/1.5117159

Cation dependent electroosmotic flow in glass nanopores

Applied Physics Letters 115, 113702 (2019); https://doi.org/10.1063/1.5116760

Lock-in Amplifiers up to 600 MHz







# Flow and mixing dynamics of phase-transforming multicomponent fluids

Cite as: Appl. Phys. Lett. 115, 104101 (2019); doi: 10.1063/1.5109889 Submitted: 13 May 2019 · Accepted: 19 August 2019 · Published Online: 3 September 2019 · Corrected: 22 April 2020









Saikat Mukherjee<sup>a)</sup> (ib) and Hector Gomez

#### **AFFILIATIONS**

School of Mechanical Engineering, Purdue University, 585 Purdue Mall, West Lafayette, Indiana 47907, USA

<sup>a)</sup>Electronic mail: mukher32@purdue.edu

#### ABSTRACT

Despite the importance of phase-transforming, multicomponent fluids in medical diagnostics, atmospheric flows, or supercavitating vehicles, our understanding of their flow and mixing dynamics is very limited. Here, we investigate two-component flows, where one of the components is an incondensable gas and the other one is a fluid that undergoes liquid-vapor phase transformations accompanied by changes in its miscibility with the gas. We derived a continuum model from a Gibbs free energy that includes gradients of the fluid density and gas concentration, leading to a generalization of the classical equations of multiphase flow hydrodynamics. High-fidelity numerical simulations of the model show a very complex interplay between flow, mixing, and phase transformations. The model predicts quantitatively the saturation vapor pressure of water for a given mixture of air and water vapor at different temperatures. When applied to the problem of collapse of cavitation bubbles, the model allows us to study the role of gas dissolved in the liquid phase in the dynamics of the collapsing bubble. Our findings on the collapse of multicomponent bubbles have a strong bearing on the multiple applications of cavitation bubbles. The proposed model opens entirely different ways to study phase-transforming multicomponent fluids.

Published under license by AIP Publishing. https://doi.org/10.1063/1.5109889

Many problems of interest in fluid dynamics involve several phases (i.e., states of matter) of the same fluid, several components (i.e., materials with different chemical compositions) in the same phase, or multiple phases and components simultaneously. Prime examples occur in atmospheric chemistry, industrial liquid sprays,<sup>2</sup> and microfluidics.3 Compared to single-phase, single-component flows, multiphase and multicomponent flows introduce two major elements of complexity—phase transformations and miscibility. These two elements are not necessarily independent because when a fluid changes its phase, it can also change its miscibility properties. Although a lot of progress has been made in understanding some particular types of multiphase flows, such as single-phase, two-component flows (e.g., oil and water in the liquid phase<sup>4</sup>) and single-component, two-phase flows (e.g., boiling and cavitation<sup>5,6</sup>), there is no general theory of multiphase flow dynamics. Recent work has also studied twophase, two-component flows using extensions of the van der Waals model. 7-10 These models have been utilized for the study of droplet motion in a shear flow, subcooled boiling on biphilic surfaces, and adiabatically induced spinodal decomposition.9 Here, we focus on flows involving one component that can undergo liquid-vapor transformations and another component that is an incondensable gas. The incondensable gas is miscible with the vapor phase of the first

component, but practically immiscible with its liquid phase. One of the simplest examples of such flows is that of air-water mixtures in which water undergoes a liquid-vapor phase transformation. These flows control fundamental processes in supercavitating vehicles, 12,13 rain formation, 14 and ocean sprays, 15 among other examples of high scientific and technological relevance. Despite their importance, these flows have remained elusive to continuum modeling. One of the reasons is the miscibility change that accompanies the water phase transformation and the radically different mathematical models that are used for miscible and immiscible flows. While miscible flows (e.g., air and water vapor) can be modeled using extensions of the Navier-Stokes equations accounting for mixing of the components and average fluid properties, <sup>16</sup> the classical approach for immiscible flows (e.g., air and liquid water) requires at least tracking an interface and considering interfacial forces, which leads to a much more complicated problem. 17 Therefore, combining the models used for mixtures of liquid water and air with the models for water vapor and air is not a viable path to derive a model for the general problem.

Here, we propose a first-principles model for air-water flows in which water can undergo liquid-vapor phase transformations. Our model builds upon the Navier-Stokes-Korteweg equations<sup>5</sup> and Wilson's mixing energy. 18 The density and the gas concentration fields

are regularized through gradient terms in the free energy. <sup>19,20</sup> We show that this enables a natural formulation of the miscibility change that accompanies phase transformations. The model accurately predicted the formation of water droplets in a mixture of air and water vapor at different temperatures. We have also used the model to solve a classical, but hitherto open problem in cavitation—how the presence of dissolved gas affects the collapse of cavitation nanobubbles. <sup>21</sup> The proposed model may also find application in other problems that involve multiple phases and components simultaneously, like diesel engines, <sup>22</sup> methane venting, <sup>23,24</sup> and focused ultrasound therapy. <sup>25</sup>

We developed our model postulating a Gibbs free energy, using standard balance laws for the mass of each component and linear momentum of the mixture, and applying the Coleman-Noll approach.<sup>26</sup> For isothermal conditions, our free-energy can be written as

$$\psi_M(\rho,c) = \psi_V(\rho) + \frac{\lambda}{2} |\nabla \rho|^2 + \frac{1}{M} B(\rho,c) + \frac{\rho \varepsilon^2}{2} |\nabla c|^2, \quad (1)$$

where  $\rho$  and c denote the density of the fluid and the concentration (mass fraction) of incondensable gas (air in what follows), respectively. The function  $\psi_V$  represents the free energy density per unit volume of a van der Waals fluid and can be expressed as  $\psi_V(\rho)$  $=R\rho\theta\log\left[\rho/(b-\rho)\right]-a\rho^2$ , where  $\theta$  is the fluid temperature (assumed constant here), R is the gas constant, and a and b are parameters of the van der Waals equation. The gradient terms in the free energy represent the interfacial surface energy density at the liquid-vapor interface and the air-water interface. They are grounded on classical work on phase transformations by van der Waals<sup>19</sup> and the groundbreaking research on mixing energies by Cahn and Hilliard. The parameters  $\lambda$ and  $\varepsilon$  can be obtained from the surface tension at the liquid-vapor interface  $(\sigma_{lv})$  and at the liquid-gas interface  $(\sigma_{lg})$ , respectively, as  $\sigma_{lv} = \int_{-\infty}^{\infty} \lambda (\nabla \rho \cdot \mathbf{n}_{lv})^2 \mathrm{d} n_{lv}^{5}$  and  $\sigma_{lg} = \int_{-\infty}^{\infty} \varepsilon^2 \rho (\nabla c \cdot \mathbf{n}_{lg})^2 \mathrm{d} n_{lg}$ , where n represents a spatial coordinate perpendicular to the relevant interface. The proof for the expression of liquid-gas surface tension is included in the supplementary material. The function  $B(\rho, c)$  is a measure of the energy of miscibility of gas in the fluid, which will be defined later. M represents a time scale for the mixing of the incondensable gas in the phase-transforming fluid. We now resort to standard balance laws for the mass of the mixture, linear momentum, and mass of incondensable gas,

$$\dot{\rho} + \rho \nabla \cdot \mathbf{v} = 0, \quad \rho \dot{\mathbf{v}} = \nabla \cdot \mathbf{T}, \quad \rho \dot{\mathbf{c}} + \nabla \cdot \mathbf{j} = 0.$$
 (2)

Here, a dot denotes the material derivative and v is the fluid velocity. The Coleman-Noll procedure<sup>26</sup> allows us to determine the Cauchy stress tensor T and the mass flux j from the condition that the Gibbs free energy must decrease in time along solutions to the balance equations. This leads to

$$T = -pI + \tau + \zeta_c + \zeta_o, \tag{3}$$

$$\mathbf{j} = -\kappa \nabla \left( \frac{1}{\rho M} \frac{\partial B}{\partial c} - \frac{\varepsilon^2}{\rho} \nabla \cdot (\rho \nabla c) \right), \tag{4}$$

where  $p=\rho\psi'_V-\psi_V$  is the van der Waals equation of state and  $\tau=\mu(\nabla v+\nabla v^T)+\eta\nabla\cdot vI$  is the classical viscous stress tensor. Here,  $\mu$  and  $\eta$  are the viscosity coefficients that will be assumed to satisfy the Stokes hypothesis, i.e.,  $\eta=-2\mu/3$ . The tensor  $\zeta_\rho=-\lambda\nabla\rho\otimes\nabla\rho+\lambda(\frac{1}{2}|\nabla\rho|^2+\rho\nabla^2\rho)I$  is the Korteweg stress which accounts for the stresses developed at the liquid-vapor interface,  $\zeta_c=-\rho\varepsilon^2\nabla c$ 

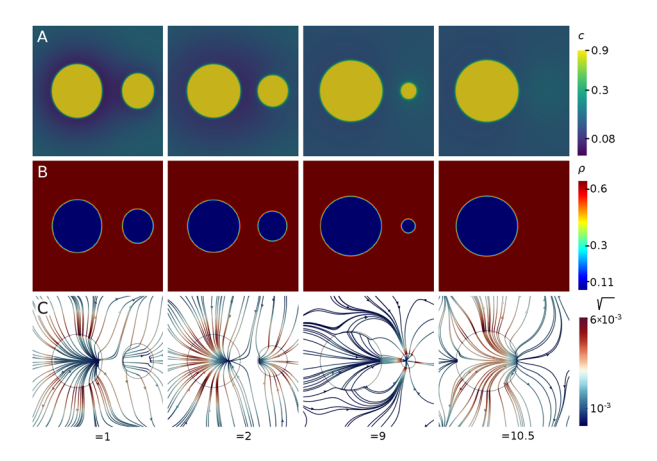
 $\otimes \nabla c + \frac{1}{M}(B - \rho \frac{\partial B}{\partial \rho})I$  is the contribution to stress emanating from the multicomponent nature of the mixture, and  $\kappa$  is a positive constant which represents a time scale for diffusion of the incondensable gas. The details of the derivation may be found in the supplementary material.

The mixing energy is defined as  $B(\rho, c) = g(\rho)f_l(c)$  $+[1-g(\rho)]f_{g}(c)$ . It can be decomposed into two parts: gas miscibility in the liquid phase and in the vapor phase. Miscibility in the liquid phase is governed by Henry's law which states that for a given temperature, solubility of a gas into a liquid is proportional to its partial pressure. Solubility of gas into the liquid is modeled with the term  $g(\rho)f_l(c)$  in  $B(\rho, c)$ . Here,  $f_l(c) = c \ln(c) + (1 - c) \ln(1 - c) - c \ln[c]$  $+\alpha_l(1-c)$ ] -(1-c) ln  $[1-c+\beta_lc]$  is a mixing energy proposed by Wilson, where the parameters  $\beta_l$  and  $\alpha_l$  determine the equilibrium concentration of gas in the liquid at vapor pressure (c1). The term  $g(\rho)=rac{
hoho_r}{
ho_lho_v}$  accounts for the increase in gas solubility in the liquid phase when pressure is increased; see data showing the compliance of the model with Henry's law in the supplementary material. Here,  $\rho_l$  and  $\rho_v$  represent the Maxwell states of the liquid and vapor phase, respectively, and are determined using common tangent constructions on the van der Waals energy density  $\psi_{V}^{19}$  The Maxwell states correspond to conditions of equal pressure and chemical potential  $(\psi'_{V})$  in the liquid and vapor phases. The miscibility of gas in the vapor phase is governed by the laws of gas mixing and is modeled in our approach by the function  $f_g(c) = c \ln(c) + (1-c) \ln(1-c) - c \ln[c + \alpha_g(1-c)]$ [-c] [1-c]  $[1-c+\beta_g c]$ ; see Ref. 18. The parameters  $\beta_g$  and  $\alpha_g$ establish the equilibrium concentration of gas in the vapor phase  $(c_v)$ . The concentration dependence of the equilibrium densities ( $\rho_v$  and  $\rho_l$ ) is taken into account by the function  $g(\rho)$  in  $B(\rho, c)$ . Depending on the nature of gas miscibility in the phase-transforming fluid, this relationship may change. For a linear relationship between  $g(\rho)$  and  $\rho$ , the Maxwell states are independent of the gas concentration; proof is included in the supplementary material. A comparison between our model and the van der Waals theory for binary mixtures under the assumption of low gas density is presented in the supplementary material.

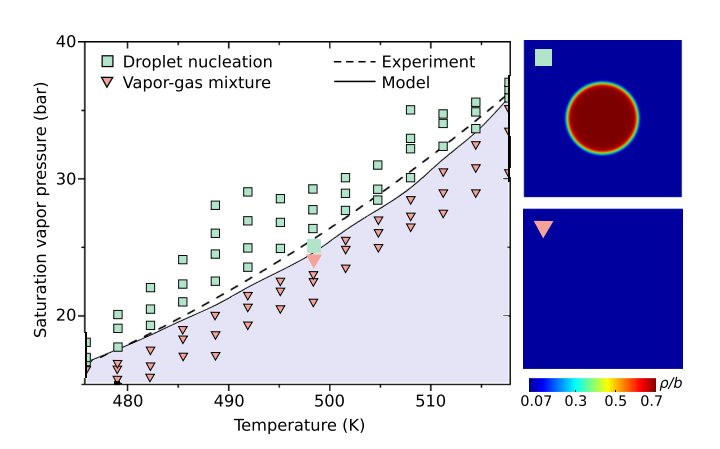
To study the model, we scale the length by  $L_0$ , mass by  $bL_0^3$ , time by  $t_D = L_0/\sqrt{ab}$ , and temperature by the critical temperature of a van der Waals fluid  $\theta_c = 8ab/(27R)$ . From this scaling, it follows that the solution depends only on the Wilson mixing energy parameters ( $\alpha_b$   $\beta_b$  $\alpha_g$ , and  $\beta_g$ ) and the following dimensionless groups: Reynolds number  $R_e = b\sqrt{ab}L_0/\mu$ , Weber number of the liquid-vapor interface  $W_e^{l\nu}$  $= aL_0^2/\lambda$ , Weber number of the liquid-gas interface  $W_e^{lg} = abL_0^2/\varepsilon^2$ , Peclet number  $P_e = L_0 \sqrt{ab}/(a\kappa)$ , and  $S_a = Mab^2$ . The dimensionless number  $S_a$  represents a balance of the mixing velocity to the liquidvapor interface velocity, whereas  $P_e$  is the ratio of the strength of advection relative to the strength of diffusion. Because surface tension and the length scale  $L_0$  are not independent in the model, we took  $L_0 = 75$  nm, such that  $\sigma_{l\nu} = \sigma_{lg} = 0.075$  N/m, which are accurate values for the corresponding surface tensions. Unless otherwise stated, for the calculations, in this paper, we used the parameters  $R_e = 1024$ ,  $W_e^{lv} = 262144, \ W_e^{lg} = 262144, P_e = 5120, \text{ and } S_a = 1000.$  The parameters of the Wilson mixing energy are also dimensionless and were taken as  $\alpha_l = \beta_g = 1$  and  $\alpha_g = \beta_l = 10^6$ . Using these parameters, the common tangent construction on the mixing energy B leads to  $c_l = 0.0975$  and  $c_v = 1 - c_l$ .

Figure 1 shows the evolution of a system containing a large vapor bubble with a small concentration of gas dissolved ( $\rho = \rho_v$ ,  $c = c_l$ ) and a smaller bubble saturated with gas ( $\rho = \rho_v$ ,  $c = c_v$ ) side by side in a pool of liquid ( $\rho = \rho_b$ ,  $c = c_l$ ) at temperature  $\theta/\theta_c = 0.85$ . Right after the simulation starts, gas is drawn from the liquid into the large vapor bubble (not shown). After this initial phase, we observe the gradual movement of gas from the smaller bubble into the larger bubble and the corresponding movement of liquid from the vicinity of the smaller bubble to occupy that space, as the equilibrium value for the density remains equal to  $\rho_v$ ; see the streamlines in Fig. 1(c) ( $t/t_D = 1$  and  $t/t_D = 2$ ). The smaller bubble keeps shrinking with time, and at equilibrium, one large bubble is formed ( $\rho = \rho_v$  and  $c = c_v$ ).

The ability of the model to predict water phase transformations in the presence of air was quantitatively evaluated by determining the saturation vapor pressure of water  $(p_{sat})$  for a given mixture of air and water vapor at different temperatures. We identified our pressure and temperature scales equating the critical pressure and temperature of a van der Waals fluid ( $p_c = ab^2/27$  and  $\theta_c = 8abR^{-1}/27$ ) to the critical pressure and temperature of water-steam mixtures ( $p_c = 220.64$  bar and  $\theta_c$  = 647.2 K); see Ref. 27. We considered air-water mixtures with uniform density such that the total pressure of the fluid according to the van der Waals equation was p = 100 bar. However, the concentration field was not uniform, and we consider a small water vapor bubble in a pool of uniform water vapor-air mixtures. We ran multiple simulations, where the mole fraction of water  $x_w$  was gradually increased, by increasing the radius of the spherical vapor bubble, in order to simulate the addition of water vapor into a partially saturated air-steam mixture. This mixture was used as an initial condition for our simulations, which evolved toward a stationary state. For very small values of  $x_w$ , we observed complete miscibility with a uniform concentration and density throughout (representative simulations are marked with triangles in Fig. 2). With the addition of more water, we obtained a general increase in density. Further addition of water leads to the formation of liquid water droplets (squares in Fig. 2). We defined the saturation pressure  $p_{sat}$  as the partial pressure of water



**FIG. 1.** Time evolution of the gas concentration (a), density (b), and streamlines (c) for two bubbles side by side in a pool of liquid at temperature  $\theta/\theta_c = 0.85$ . The Maxwell states  $(\rho_c/b = 0.106$  and  $\rho_c/b = 0.602$ ), which define equilibrium conditions, are not altered by the distribution of incondensable gas. For clarity, we only show the central part of the computational domain. The plot shows a very complex interplay between phase transformations and miscibility.



**FIG. 2.** Saturation vapor pressure for air-water mixtures. The model results (solid line) accurately match the experiments  $^{27}$  (dashed line). The model results were obtained by running dynamic simulations (each one marked with a symbol) with different temperatures and water mole fractions. The magnified snapshots showcase steady state density distributions for  $\theta=498.42\,\mathrm{K}$  ( $\rho_v/b=0.0668$  and  $\rho/b=0.6669$ ) and  $\rho=100\,\mathrm{bar}$ , corresponding to  $\mathrm{x_w}$  values of 0.3420 and 0.3490 which are representative of density distribution for unsaturated and saturated conditions, respectively.

corresponding to the smallest value of  $x_w$  for which liquid droplets are observed, that is,  $p_{sat} = px_w^{\min}$ . Several such families of simulations were run for different values of  $\theta$  in order to determine the saturation vapor pressure curve. Figure 2 shows that the values calculated using the model are very close to those obtained experimentally.<sup>27</sup>

Another important application of our model is the dynamics of cavitation nanobubbles.<sup>28-32</sup> The field has been traditionally divided into pure vapor bubbles<sup>5</sup> and pure gas bubbles.<sup>33</sup> However, the study of the general problem in which vapor and an incondensable gas interact chemically and mechanically has remained qualitative<sup>21</sup> due to the absence of a firm theoretical framework. To study this problem, we initially ran simulations with a uniform gas concentration of  $c = c_l$ throughout. A vapor bubble with a radius  $R_{eq}$  initially in equilibrium was subjected to a far field overpressure  $\Delta p = p_{\infty} - p_b$ . The pressures  $p_{\infty}$  and  $p_b$  were set using their corresponding densities  $\rho_{\infty}$  and  $\rho_b$ according to the van der Waals equation of state. We took  $\theta/\theta_c = 0.85, R_{eq}/L_0 = 0.05, \rho_{\infty}/b = 0.7028, \text{ and } \rho_b/b = 0.0800.$  We show snapshots of the time evolution of the density [Fig. 3(a)] and concentration of incondensable gas [Fig. 3(b)]. Figures 3(c) and 3(d) show the time evolution of the pressure and gas concentration (insets) in the radial (*r*) direction. Before bubble collapse ( $t/t_D \approx 0.180$ ), we can observe a shrinking bubble with large density and pressure gradients at the liquid-vapor interface and a large amount of incondensable gas in its interior, which was quickly drawn from the liquid phase due to the higher miscibility of gas in the vapor phase (compare the snapshots of the gas concentration at times  $t/t_D = 0$  and  $t/t_D = 0.14$ ). During the precollapse phase, the model predicts a strong compression wave and an increase in the pressure at the bubble interface that reaches its maximum at the collapse time; see Fig. 3(c). The postcollapse phase is marked by the propagation of a rarefaction wave away from the bubble [Fig. 3(d)]. The speed of this rarefaction wave is much higher than that of the incoming compression wave which was responsible for the bubble collapse. The pressure peaks in the postcollapse phase follow a power law relationship similar to that proposed by Hickling-Plesset.<sup>3</sup>

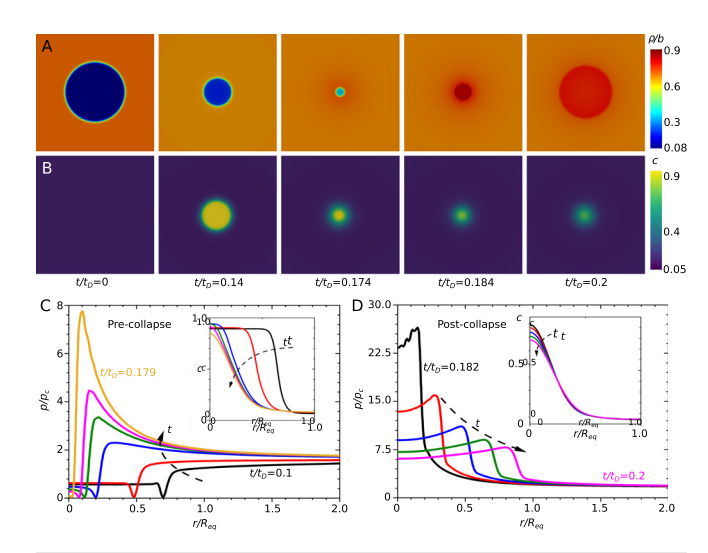


**FIG. 3.** Time evolution of density (a) and gas concentration (b) for a collapsing bubble. Time evolution of the pressure and gas concentration (insets) along the radial direction (*r*) in the precollapse (c) and postcollapse (d) stages.

To compare the results reported in Fig. 3 with those of an identical situation but without incondensable gas, we repeated our simulation taking c = 0 throughout. We focused on two quantities of interest: the time evolution of the bubble radius  $(R_b)$  and the interface Mach number. To define the radius, we identified the bubble boundary as the curve along which the pressure gradient was maximum. The Mach number was defined as  $M_a = |v|/\sqrt{\gamma \theta R b^2 (\rho - b)^{-2}} - 2a \rho$ , where  $\gamma$ = 1.4 is the adiabatic constant. The data in Fig. 4 show three major differences produced by the presence of incondensable gas: (i) bubble collapse is slower ( $t/t_D \approx 0.180$  vs  $t/t_D \approx 0.162$ ), (ii) the Mach number at the interface is lower ( $M_a \approx 0.593$  vs  $M_a \approx 0.633$ ), and (iii) the minimum bubble radius is greater than zero. The results show that the presence of incondensable gas inhibits bubble collapse, which is consistent with Ref. 21. This is expected because vapor converts into liquid with the application of sufficient pressure, but gas miscibility in the liquid at a particular temperature and pressure is limited by Henry's law. From Fig. 4, it is also clear that the final phase of bubble collapse is characterized by rapid compression. This can be explained by the sharp increase in the pressure at the interface right before bubble collapse; see Fig. 3(c). The high pressure promotes conversion from the

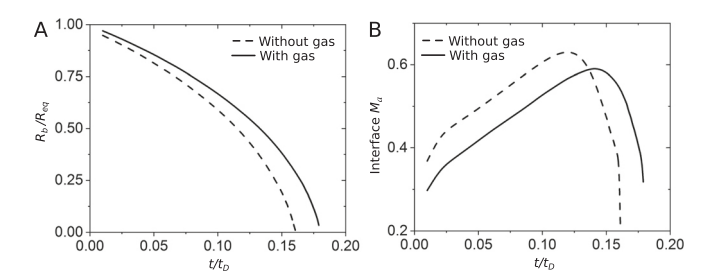


**FIG. 4.** (a) Time evolution of vapor bubble radii  $R_b/R_{eq}$  with and without incondensable gas. (b) Time evolution of the interface Mach number with and without incondensable gas.

vapor phase to the liquid phase. Although the rate of decrease in the bubble radius is slower when incondensable gas is present, it still accelerates in the later stages owing to enhanced gas miscibility in the liquid with an increase in pressure.

Because the gas is practically immiscible with the liquid phase and highly miscible in vapor, even small amounts of gas dissolved in the liquid can produce changes in the dynamics of bubble collapse. To study this, we carried out additional simulations varying the initial degree of saturation of the fluid  $(\phi)$  and the dimensionless parameter  $S_a$  which controls the time scale of the mixing process because different gases have different characteristic time scales of mixing in a vapor bubble.<sup>34</sup> As we do not have (at the scales studied here) experimental data to estimate the value of  $S_a$ , we show simulations for a wide range of values. A vapor bubble with some gas ( $\rho/b = 0.0800$  and  $c = c_l$ ) was placed in a bath of liquid with varying concentrations of dissolved gas  $(\rho/b = 0.7028$  and  $c = \phi c_l$ ). We applied an excess far field pressure identical to that used in the previous simulation and studied the time evolution of the average concentration of gas inside the bubble  $(c_b)$ . For the parameters used in the simulation corresponding to the thickest (black) curve in Fig. 5, we can partition the process into four stages marked in the figure with different colors. In the first stage,  $c_h$  increases quickly because gas is being drawn from the liquid into the bubble. Also, the low miscibility of gas into the liquid maintains the gas practically confined into the shrinking bubble, leading to an increase in  $c_b$ . In the second stage,  $c_b$  increases more slowly. Because the bubble is still shrinking at a fast rate, this can only be explained by the dissolution of gas into the liquid. This is a consequence of the large pressure in the liquid phase [cf. with Fig. 3(c)], which according to Henry's law increases the solubility of gas into the liquid. The data show that this behavior is naturally captured by the model. The plateau in  $c_h$  is reached faster for larger  $\phi$  and smaller  $S_a$  because in this parameter range, the gas can move more easily into the bubble. In the third stage,  $c_h$  grows again because the size of the bubble is decreasing very quickly right before the collapse and the pressure is not high enough to allow for dissolution of all the excess gas into the liquid. In the fourth stage, due to the dramatic increase in the pressure right before bubble collapse, the liquid phase becomes much more soluble and  $c_b$  decreases quickly. In all, the simulations show a very complex interplay between mass conservation, linear momentum balance, and solubility which cannot be quantitatively understood without a computational model.

In conclusion, we have presented a model of two-component flows, where one of the components is an incondensable gas and the other one is a fluid that undergoes liquid-vapor transformations. The

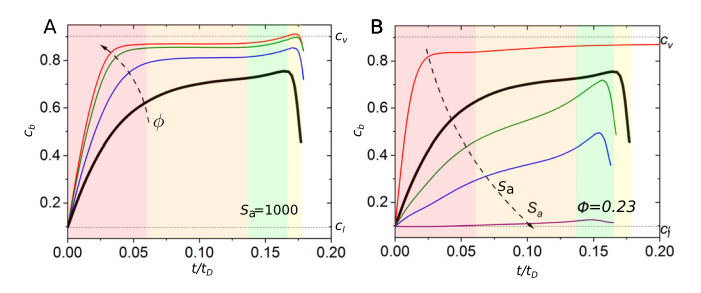


**FIG. 5.** Time evolution of the average concentration of gas in the bubble  $(c_b)$ . (a) Results for  $S_a=1000$  and  $\phi=0.23,\,0.43,\,0.64,\,$  and 1.21. (b) Results for  $\phi=0.23$  and  $S_a=400\,000,\,5000,\,1000,\,5000,\,$  and 200.

model is derived from a higher-order Gibbs free energy that includes gradients of the density and gas concentration, constituting a generalization of classical equations of multiphase hydrodynamics, which is consistent with recent effort in porous media flows. 24,35 The model predicts quantitatively the saturation vapor pressure of water for a given mixture of air and water vapor at different temperatures. The model highlights the importance of dissolved gas in the collapse of cavitation bubbles. In this context, the extension of the proposed model to nonisothermal conditions is particularly promising for the study of the postcollapse phase. This extension can be done by factoring the temperature dependence of the equilibrium concentrations into the model, by suitably varying the parameters  $\alpha_g$ ,  $\beta_g$ ,  $\alpha_b$  and  $\beta_l$  with the temperature and adding an equation for conservation of energy. After the collapse, the concentration and density at the interface become very diffuse, making it difficult to define a sharp bubble boundary. This suggests that classical models based on ordinary differential equations for the bubble radius may be inadequate in the multicomponent, multiphase problem even if the solution remains axisymmetric. We believe that our model can also have a significant impact on other problems that involve simultaneous several phases and several components, for example, diesel engines,<sup>22</sup> methane venting, 23,24 and focused ultrasound therapy. 2

See the supplementary material for the details of the derivation of our model starting from the free energy formulation proposed in (1), applying the Coleman-Nole procedure,  $^{26}$  a derivation for  $\sigma_{lg}$ , details of the comparison of the presented model with the van der Waals theory for binary mixtures under the assumption of low gas density, the details regarding nondimensionalization, numerical procedure followed for solving the family of equations (2), and a derivation for speed of sound in van der Waals fluids.

We gratefully acknowledge funding for this research provided by the National Science Foundation under contract CBET 1805817.

## REFERENCES

- <sup>1</sup>M. Shrivastava, M. O. Andreae, P. Artaxo, H. M. Barbosa, L. K. Berg, J. Brito, J. Ching, R. C. Easter, J. Fan, J. D. Fast *et al.*, "Urban pollution greatly enhances formation of natural aerosols over the amazon rainforest," Nat. Commun. **10**, 1046 (2019).
- <sup>2</sup>Y. Wang, X. Liu, K.-S. Im, W.-K. Lee, J. Wang, K. Fezzaa, D. L. Hung, and J. R. Winkelman, "Ultrafast x-ray study of dense-liquid-jet flow dynamics using structure-tracking velocimetry," Nat. Phys. 4, 305 (2008).
- <sup>3</sup>G. M. Whitesides, "The origins and the future of microfluidics," Nature 442, 368 (2006).
- <sup>4</sup>J. Lu and G. Tryggvason, "Direct numerical simulations of multifluid flows in a vertical channel undergoing topology changes," Phys. Rev. Fluids 3, 084401 (2018).
- <sup>5</sup>F. Magaletti, L. Marino, and C. M. Casciola, "Shock wave formation in the collapse of a vapor nanobubble," Phys. Rev. Lett. **114**, 064501 (2015).
- <sup>6</sup>J. Liu, C. M. Landis, H. Gomez, and T. J. Hughes, "Liquid-vapor phase transition: Thermomechanical theory, entropy stable numerical formulation, and boiling simulations," Comput. Methods Appl. Mech. Eng. 297, 476–553 (2015).
- <sup>7</sup>J. Liu, G. Amberg, and M. Do-Quang, "Diffuse interface method for a compressible binary fluid," Phys. Rev. E **93**, 013121 (2016).

- <sup>8</sup>A. Onuki, "Henry's law, surface tension, and surface adsorption in dilute binary mixtures," J. Chem. Phys. **130**, 124703 (2009).
- <sup>9</sup>A. Onuki, "Dynamic Van der Waals theory," Phys. Rev. E 75, 036304 (2007).
- <sup>10</sup> A. G. Lamorgese, D. Molin, and R. Mauri, "Phase field approach to multiphase flow modeling," Milan J. Math. 79, 597–642 (2011).
- <sup>11</sup>B. Shen, J. Liu, J. Shiomi, G. Amberg, M. Do-Quang, M. Kohno, K. Takahashi, and Y. Takata, "Effect of dissolved gas on bubble growth on a biphilic surface: A diffuse-interface simulation approach," Int. J. Heat Mass Transfer 126, 816–829 (2018)
- <sup>12</sup>T. T. Truscott, B. P. Epps, and J. Belden, "Water entry of projectiles," Annu. Rev. Fluid Mech. 46, 355–378 (2014).
- <sup>13</sup>S. L. Ceccio, "Friction drag reduction of external flows with bubble and gas injection," Annu. Rev. Fluid Mech. 42, 183–203 (2010).
- 14. W. W. Grabowski and L.-P. Wang, "Growth of cloud droplets in a turbulent environment," Annu. Rev. Fluid Mech. 45, 293–324 (2013).
- <sup>15</sup>F. Veron, "Ocean spray," Annu. Rev. Fluid Mech. 47, 507–538 (2015).
- <sup>16</sup>A. W. Cook and P. E. Dimotakis, "Transition stages of Rayleigh-Taylor instability between miscible fluids," J. Fluid Mech. 443, 69–99 (2001).
- <sup>17</sup>J. Lu, A. Fernández, and G. Tryggvason, "The effect of bubbles on the wall drag in a turbulent channel flow," Phys. Fluids 17, 095102 (2005).
- <sup>18</sup>G. M. Wilson, "Vapor-liquid equilibrium. XI. A new expression for the excess free energy of mixing," J. Am. Chem. Soc. 86, 127–130 (1964).
- 19 J. Rowlinson, "Translation of JD van der waals' 'The thermodynamik theory of capillarity under the hypothesis of a continuous variation of density'," J. Stat. Phys. 20, 197–200 (1979).
- <sup>20</sup>J. W. Cahn and J. E. Hilliard, "Free energy of a nonuniform system. I. Interfacial free energy," J. Chem. Phys. 28, 258–267 (1958).
- <sup>21</sup>A. Prosperetti, "Vapor bubbles," Annu. Rev. Fluid Mech. **49**, 221–248 (2017).
- <sup>22</sup>M. Gorokhovski and M. Herrmann, "Modeling primary atomization," Annu. Rev. Fluid Mech. 40, 343–366 (2008).
- <sup>23</sup>M. Sipilä, T. Berndt, T. Petäjä, D. Brus, J. Vanhanen, F. Stratmann, J. Patokoski, R. L. Mauldin, A.-P. Hyvärinen, H. Lihavainen *et al.*, "The role of sulfuric acid in atmospheric nucleation," Science 327, 1243–1246 (2010).
- <sup>24</sup>X. Fu, L. Cueto-Felgueroso, and R. Juanes, "Nonequilibrium thermodynamics of hydrate growth on a gas-liquid interface," Phys. Rev. Lett. 120, 144501 (2018).
- 25C. C. Coussios and R. A. Roy, "Applications of acoustics and cavitation to non-invasive therapy and drug delivery," Annu. Rev. Fluid Mech. 40, 395–420
- <sup>26</sup>B. D. Coleman and W. Noll, "The thermodynamics of elastic materials with heat conduction and viscosity," Arch. Ration. Mech. Anal. 13, 167–178 (1963).
- <sup>27</sup>A. Harvey, A. Peskin, and S. Klein, "NIST/ASME steam properties," NIST Standard Reference Database 10 (NIST, 1997).
- <sup>28</sup>E. A. Neppiras, "Acoustic cavitation," Phys. Rep. **61**, 159–251 (1980).
- <sup>29</sup>P. Prentice, A. Cuschieri, K. Dholakia, M. Prausnitz, and P. Campbell, "Membrane disruption by optically controlled microbubble cavitation," Nat. Phys. 1, 107 (2005).
- <sup>30</sup>C.-D. Ohl, M. Arora, R. Ikink, N. De Jong, M. Versluis, M. Delius, and D. Lohse, "Sonoporation from jetting cavitation bubbles," Biophys. J. 91, 4285–4295 (2006).
- <sup>31</sup>S. D. Hyman, T. J. W. Lazio, N. E. Kassim, P. S. Ray, C. B. Markwardt, and F. Yusef-Zadeh, "A powerful bursting radio source towards the galactic centre," Nature 434, 50 (2005).
- 32C. E. Brennen, Cavitation and Bubble Dynamics (Cambridge University Press, 2014)
- 33R. Hickling and M. S. Plesset, "Collapse and rebound of a spherical bubble in water," Phys. Fluids 7, 7–14 (1964).
- <sup>34</sup>R. Hiller, K. Weninger, S. J. Putterman, and B. P. Barber, "Effect of noble gas doping in single-bubble sonoluminescence," Science 266, 248–250 (1994).
- 35L. Cueto-Felgueroso and R. Juanes, "Macroscopic phase-field model of partial wetting: Bubbles in a capillary tube," Phys. Rev. Lett. 108, 144502 (2012).